



**CHALMERS**  
UNIVERSITY OF TECHNOLOGY

## **Simplified Kinetic Model for NH<sub>3</sub>-SCR Over Cu-CHA Based on First-Principles Calculations**

Downloaded from: <https://research.chalmers.se>, 2022-12-10 11:03 UTC

Citation for the original published paper (version of record):

Feng, Y., Creaser, D., Grönbeck, H. (2022). Simplified Kinetic Model for NH<sub>3</sub>-SCR Over Cu-CHA Based on First-Principles Calculations. *Topics in Catalysis*.  
<http://dx.doi.org/10.1007/s11244-022-01711-5>

N.B. When citing this work, cite the original published paper.



# Simplified Kinetic Model for NH<sub>3</sub>-SCR Over Cu-CHA Based on First-Principles Calculations

Yingxin Feng<sup>1</sup> · Derek Creaser<sup>2</sup> · Henrik Grönbeck<sup>1</sup>

Accepted: 30 September 2022  
© The Author(s) 2022

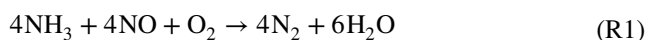
## Abstract

Selective catalytic reduction with ammonia as reducing agent (NH<sub>3</sub>-SCR) is an efficient technology to control NO<sub>x</sub> emission during oxygen excess. Catalysts based on Cu-chabazite (Cu-CHA) have shown good performance for NH<sub>3</sub>-SCR with high activity and selectivity at low temperature and good hydrothermal stability. Here, we explore a first-principles based kinetic model to analyze in detail which reaction steps that control the selectivity for N<sub>2</sub> and the light-off temperature. Moreover, a simplified kinetic model is developed by fitting lumped kinetic parameters to the full model. The simplified model describes the reaction with high accuracy using only five reaction steps. The present work provides insight into the governing reaction mechanism and stimulates design of knowledge-based Cu-CHA catalysts for NH<sub>3</sub>-SCR.

**Keywords** First-principles microkinetic modeling · NH<sub>3</sub>-SCR · Cu-CHA · Parameter evaluation

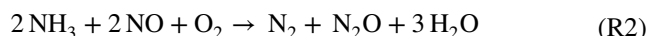
## 1 Introduction

Copper-exchanged small-pore zeolites with chabazite structure (Cu-CHA), are state-of-the-art catalysts for ammonia assisted selective catalytic reduction (NH<sub>3</sub>-SCR) in emission control of diesel exhaust [1]. Thanks to low-temperature activity, high selectivity for N<sub>2</sub>, and hydrothermal stability [2–4], Cu-CHA is a preferred catalyst for NH<sub>3</sub>-SCR and has matured to commercial application. NO is the main NO<sub>x</sub> component in diesel exhaust and selective reduction of NO to N<sub>2</sub> with NH<sub>3</sub> is known as the standard-SCR reaction:



Each NO couples with one NH<sub>3</sub> and O<sub>2</sub> is needed to complete the stoichiometry.

Although high selectivity for N<sub>2</sub> has been achieved over Cu-CHA, a small amount of N<sub>2</sub>O is formed under NH<sub>3</sub>-SCR conditions [5, 6]. N<sub>2</sub>O is an undesired by-product and has received wide attention due to its high greenhouse potential. An overall reaction where N<sub>2</sub>O is formed is:



To further enhance the selectivity for N<sub>2</sub> over Cu-CHA, understanding of the reaction mechanism for N<sub>2</sub>O formation during NH<sub>3</sub>-SCR is desired. Advancing the atomic understanding of the reactions could in this respect guide the development of next generations of catalysts. For this purpose we have developed first-principles microkinetic models for low-temperature conditions [7] based on multi-site reaction mechanisms [8].

The proposed reaction cycle for NH<sub>3</sub>-SCR is shown in Fig. 1. Under the reaction condition of standard NH<sub>3</sub>-SCR, Cu ions are at low temperatures solvated by NH<sub>3</sub> and mainly present as [Cu(NH<sub>3</sub>)<sub>2</sub>]<sup>+</sup> species [9–11]. O<sub>2</sub> adsorption is a key step in the reaction and a pair of [Cu(NH<sub>3</sub>)<sub>2</sub>]<sup>+</sup> complexes is needed for O<sub>2</sub> adsorption, forming a Cu-peroxo complex, [Cu<sub>2</sub>(NH<sub>3</sub>)<sub>4</sub>O<sub>2</sub>]<sup>2+</sup> [9, 12, 13]. The oxidation state of Cu changes from +1 to +2 [14] during O<sub>2</sub> adsorption, which allows the adsorption of NO and NH<sub>3</sub> at relevant temperatures. Upon NO adsorption (reaction 2), NO reduction

✉ Yingxin Feng  
yingxin@chalmers.se

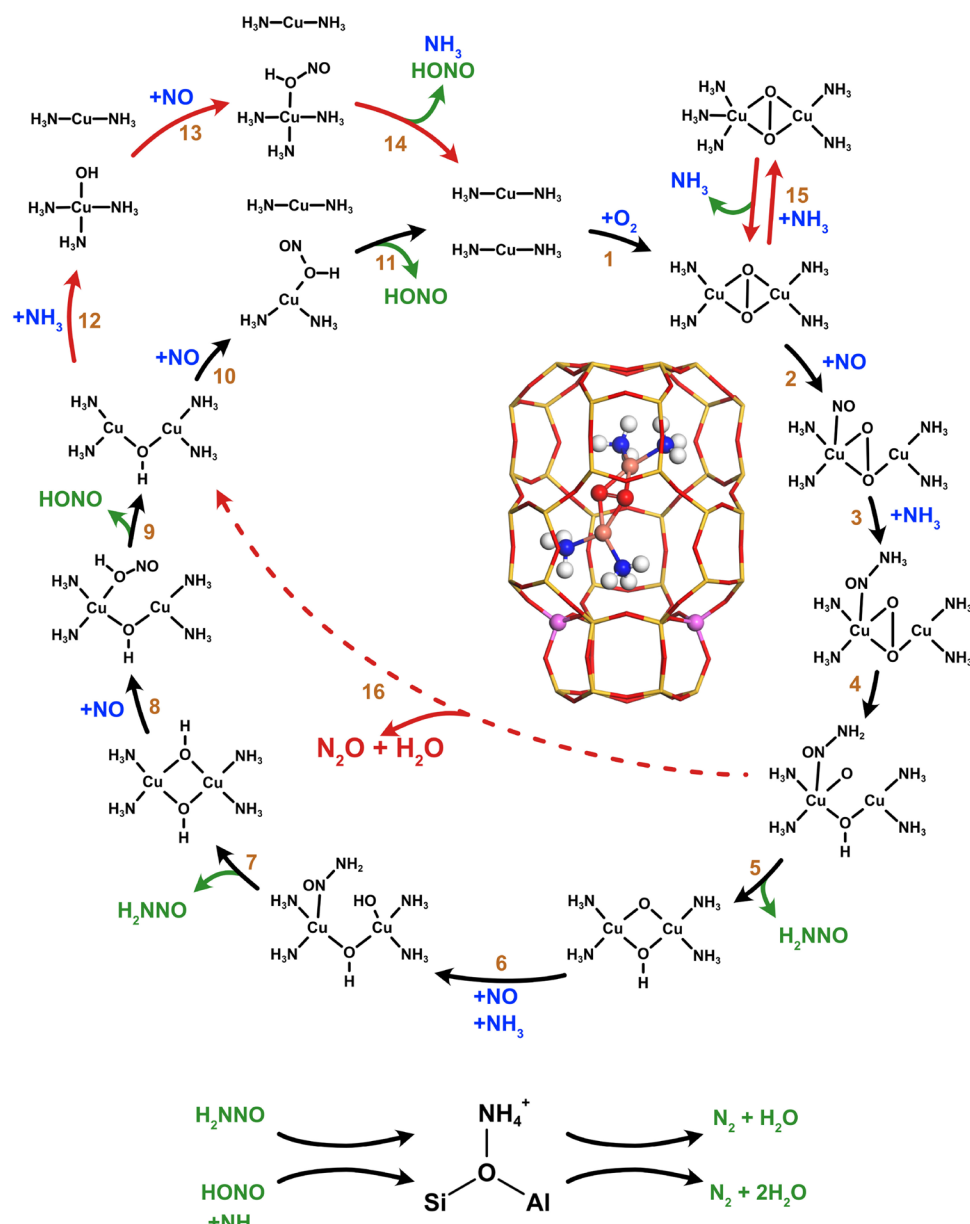
✉ Henrik Grönbeck  
ghj@chalmers.se

Derek Creaser  
derek.creaser@chalmers.se

<sup>1</sup> Department of Physics and Competence Centre for Catalysis, Chalmers University of Technology, 41296 Göteborg, Sweden

<sup>2</sup> Department of Chemistry and Chemical Engineering, Chalmers University of Technology, 41296 Göteborg, Sweden

**Fig. 1** Proposed reaction cycle for low-temperature  $\text{NH}_3$ -SCR over Cu-CHA and the side view of the chabazite cages showing the Al positions in the six-membered ring which also includes the  $[\text{Cu}_2(\text{NH}_3)_4(\text{O}_2)]^{2+}$  complex. Atom color codes: Cu (bronze), Si (yellow), Al (pink), O (red), N (blue), and H (white). Adapted from Ref. [7]



proceeds via formation of  $\text{H}_2\text{NNO}$  and  $\text{HONO}$  intermediates. The intermediates in this model are assumed to diffuse from the Cu-sites to neighboring Brønsted acid sites where they decompose into  $\text{N}_2$  and  $\text{H}_2\text{O}$  by reactions with  $\text{NH}_3$  [7, 8]. Unwanted  $\text{N}_2\text{O}$  formation (reaction 16) may occur via  $\text{H}_2\text{NNO}$  decomposition over the Cu-sites [7, 15]. The selectivity for  $\text{N}_2$  depends on the competition between the diffusion of  $\text{H}_2\text{NNO}$  from the  $[\text{Cu}_2(\text{NH}_3)_4\text{OOH}]^{2+}$  complex to the Brønsted acid sites (reaction 5) and the direct decomposition of  $\text{H}_2\text{NNO}$  on the complex (reaction 16). If  $\text{H}_2\text{NNO}$  desorbs from the Cu complex, the reaction will follow the outer cycle and give an overall reaction as R1. However, for the case that  $\text{H}_2\text{NNO}$  decomposes over the Cu complex, the reaction will follow the dashed route which forms  $\text{N}_2\text{O}$  as R2.

$\text{NO}$  conversion to either  $\text{N}_2$  or  $\text{N}_2\text{O}$  may be inhibited by  $\text{NH}_3$  adsorption on the  $[\text{Cu}_2(\text{NH}_3)_4\text{O}_2]^{2+}$  complex (reaction 15). The  $\text{NH}_3$  adsorption is in the reaction cycle yielding  $[\text{Cu}_2(\text{NH}_3)_5\text{O}_2]^{2+}$ , however, it may also lead to decomposition of the peroxo complex [7, 13]. Note that  $\text{NH}_3$  has four different roles in the catalytic cycle shown in 1.  $\text{NH}_3$  is simultaneously i) a ligand that enables facile Cu-mobility, ii) a reactant, iii) adsorbed at the Brønsted acid site forming  $\text{NH}_4^+$ , which is the active site for  $\text{H}_2\text{NNO}$  and  $\text{HONO}$  conversion, and iv) an inhibitor that prevents the adsorption of  $\text{NO}$  on the Cu-peroxo complex [7].

In this contribution, we further investigate factors that control the selectivity for  $\text{N}_2$  and the  $\text{NH}_3$  inhibition. For the selectivity for  $\text{N}_2$ , the competition between reaction 5 and

16 is discussed in detail. It is revealed that a reduction of the  $\text{H}_2\text{NNO}$  desorption energy on the Cu-peroxo enhances the selectivity for  $\text{N}_2$ , which is one possibility to further improve the catalyst performance. The  $\text{NH}_3$  inhibition is discussed in relation to the onset of the low-temperature activity and different mechanisms to exit the blocked state are presented. In addition to the mechanistic aspects, we show that the detailed microkinetic model with 18 steps can be replaced with a simplified model with only 5 steps, which accurately reproduce the results of the full model.

## 2 Computational Methods

### 2.1 Density Functional Theory Calculations

Spin-polarized density functional theory (DFT) calculations are carried out with the Vienna Ab-initio Simulation Package (VASP) [16–19], using the gradient-corrected Perdew-Burke-Ernzerhof (PBE) functional [20] augmented with a Hubbard-U term of 6 eV for the Cu 3d states as proposed in previous studies [21, 22]. To account for the van der Waals interactions of the molecules in the zeolites, Grimme-D3 corrections have been applied [23, 24]. The valence electrons are described with a plane wave basis set with a cutoff energy of 480 eV, whereas the interaction between the valence and the cores are described using the projector augmented wave (PAW) method [25, 26]. The k-point sampling is restricted to the gamma point. The Climbing Image Nudged Elastic Band (CI-NEB) method [27, 28] is employed to calculate the reaction barriers and the transition states are confirmed by vibrational analyses. *Ab initio* molecular dynamics (AIMD) simulations are performed in the canonical (NVT) ensemble [29, 30] at 300 K to probe the potential energy surface and low energy configurations are obtained by structural relaxation from the trajectories. The experimental lattice constants ( $\alpha = \beta = \gamma = 94.2^\circ$ ,  $a = b = c = 9.42 \text{ \AA}$ ) are used for the CHA unit cell.

### 2.2 Microkinetic Modeling

For the microkinetic modeling, MATLAB R2018b is used with the `ode23s` solver to numerically integrate the system of differential equations until steady-state is reached. The full model includes 16 reaction steps as shown in Fig. 1 and two steps over the Brønsted acid sites [7]. The kinetic parameters for the full model are published elsewhere [7].

Here, a simplified model with only five reaction steps is developed. The simplified model uses lumped reaction steps with kinetic parameters estimated by fitting to the detailed model. The `simulannealbnd` optimizer is applied to perform the non-linear regression. An objective function ( $\tau$ ) for the parameter estimation is chosen as the normalized

difference between the results from the detailed model (denoted ref) and the simplified model (denoted sim):

$$\tau = \sum_T \left( \sqrt{\left( \frac{\text{TOF}_{\text{sim}}}{\text{TOF}_{\text{ref}}} - 1 \right)^2} + w \sqrt{\left( \frac{S_{\text{sim}}}{S_{\text{ref}}} - 1 \right)^2} \right) \quad (1)$$

where the turnover frequency of NO and selectivity for  $\text{N}_2$  are denoted TOF and S, respectively. A weighting factor ( $w = 10$ ) is added to the part of the normalized difference in selectivity to enhance the importance of the selectivity.

## 3 Results and Discussion

### 3.1 Steps Controlling the Selectivity and Light-Off Temperature

Here we further investigate the steps that previously [7] were found to determine the selectivity for  $\text{N}_2$  and the light-off temperature for  $\text{NH}_3$ -SCR over Cu-CHA. The aim is to gain deeper insights into the mechanisms that control these steps and reveal how they influence the kinetic behavior.

#### 3.1.1 Selectivity for $\text{N}_2$

In the kinetic model [7], the selectivity for  $\text{N}_2$  depends on the ratio between reaction rate of reaction 5 and reaction 16. Reaction 5 contains desorption of  $\text{H}_2\text{NNO}$  from  $[\text{Cu}_2(\text{NH}_3)_4\text{OOH}]^{2+}$  and diffusion through an eight membered ring in the zeolite to a Brønsted acid site. Previous calculations show that  $\text{H}_2\text{NNO}$  desorption is associated with a barrier of 0.3 eV and that the barrier for diffusion is about 0.1 eV. The effective barrier for reaction 5 is, thus, set to 0.3 eV. For reaction 16, the decomposition of  $\text{H}_2\text{NNO}$  over  $[\text{Cu}_2(\text{NH}_3)_4\text{OOH}]^{2+}$  forming  $\text{N}_2\text{O}$ ,  $\text{H}_2\text{O}$  and  $[\text{Cu}_2(\text{NH}_3)_4\text{OH}]^{2+}$  may involve changes in the spin configuration [15], which makes it challenging to determine accurately the reaction barrier. Here we have considered the case where the spin state of the Cu-cations are preserved along the reaction path.

To investigate how the selectivity depends on the ratio between the barrier of reaction 5 and 16, we performed simulations where the ratio was changed, Fig. 2. In the simulations, the forward reaction barrier of Reaction 5 ( $E_{5f}$ ) was fixed to 0.3 eV, whereas the forward reaction barrier of reaction 16 ( $E_{16f}$ ) was changed from 0.3 to 0.42 eV.

The selectivity for  $\text{N}_2$  depends strongly on the  $E_{16f}/E_{5f}$  ratio at low ratios. The selectivity at 373 K increase from 80% to 95% when the ratio increase from 1 to 1.2. The dependence is less pronounced at higher  $E_{16f}/E_{5f}$  ratios and the effect of increasing the ratio on the selectivity becomes small for cases when the ratio is larger than 1.3.  $E_{16f}$  is close to the calculated DFT barrier when the ratio is 1.3. The

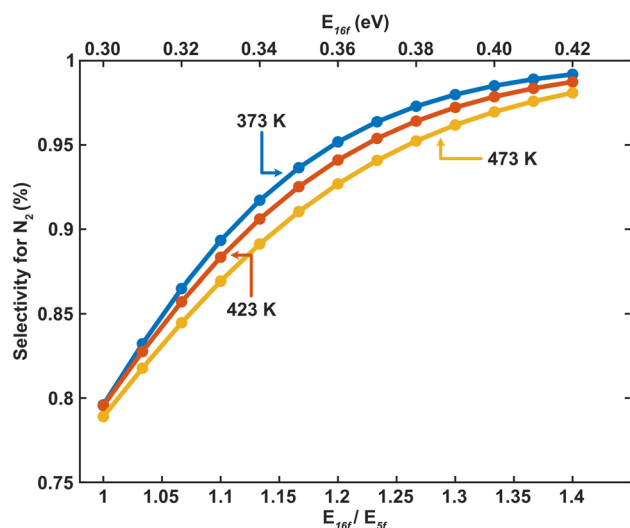


**Fig. 2** The selectivity for  $N_2$  for different ratios between the barrier of reaction 5 and reaction 16 at 373, 423, and 473 K, respectively

strong dependence of the selectivity on the  $E_{16f}/E_{5f}$  ratio shows that lowering the  $H_2NNO$  desorption energy could lead to a higher selectivity for  $N_2$ . The desorption energy could potentially be effected by the Al-distribution [31].

### 3.1.2 Site Blocking and Light-Off Temperature

Adsorption of  $NH_3$  instead of  $NO$  on the  $[Cu_2(NH_3)_4(O_2)]^{2+}$  complex blocks the site for the SCR-reaction [7]. The inhibiting effect of  $NH_3$  is severe as the adsorption energy of  $NH_3$  is higher than that of  $NO$ ;  $-0.98$  eV as compared to  $-0.70$  eV. It was in Ref. [7] shown that the light-off temperature of the SCR reaction is determined by the  $NH_3$  inhibition as the temperature should be high enough to facilitate  $NH_3$  desorption. Adsorption of  $NH_3$  on  $[Cu_2(NH_3)_4(O_2)]^{2+}$  has also been observed experimentally using X-ray absorption spectroscopy (XAS) [13] where it was suggested that the  $[Cu_2(NH_3)_5(O_2)]^{2+}$  complex dissociates into two Cu complexes  $[Cu(NH_3)_3O_2]^+$  and  $[Cu(NH_3)_2]^+$ . The energy difference between  $[Cu_2(NH_3)_5(O_2)]^{2+}$  and  $[Cu(NH_3)_3(O_2)]^+$  with  $[Cu(NH_3)_2]^+$  was in Ref. [7] calculated to be only  $0.04$  eV. In the kinetic model [7], the  $NH_3$  inhibition step was considered as adsorption onto  $[Cu_2(NH_3)_5O_2]^{2+}$  (reaction 15 in Fig. 1).

It could be noted that molecular crystals have been synthesized with the  $Cu_2O_2$  unit coordinated to six nitrogen-based ligands [32], which indicates that adsorption of additional  $NH_3$  could possibly form  $[Cu_2(NH_3)_6O_2]^{2+}$  during  $NH_3$ -SCR in CHA. To investigate the effect of  $NH_3$  inhibition in detail, we have here performed DFT calculations for sequential  $NH_3$  adsorption onto the  $[Cu_2(NH_3)_4O_2]^{2+}$  complex, Fig. 3.  $NH_3$  can adsorb on the Cu site of  $[Cu_2(NH_3)_4O_2]^{2+}$  with an adsorption energy of  $-0.98$  eV as shown in Fig. 3(B).

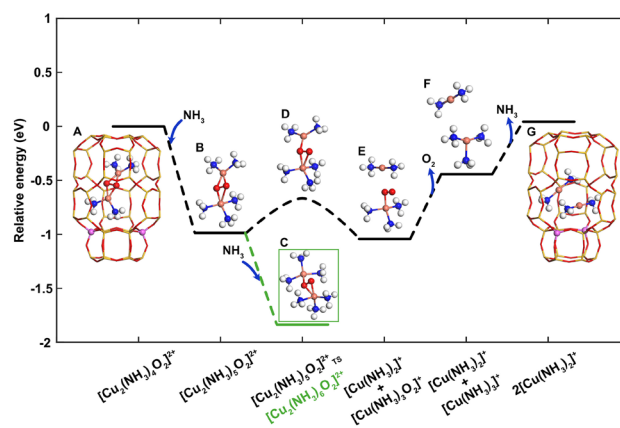


**Fig. 3** The potential energy landscape of  $NH_3$  adsorption over  $[Cu_2(NH_3)_4O_2]^{2+}$  complex in CHA. Atomic color codes are the same as those in Fig. 1

After forming structure B, an additional  $NH_3$  can adsorb with an adsorption energy of  $-0.85$  eV on the other Cu-cation forming  $[Cu_2(NH_3)_6O_2]^{2+}$  (structure C in Fig. 3). Without additional  $NH_3$ , structure B could dissociate into structure E via the transition state D. The barrier for dissociation is calculated to be  $0.33$  eV. Configuration E is consistent with the experimental interpretation of the XAS spectra [13]. As the complex has dissociated,  $O_2$  and  $NH_3$  bonded with the Cu-cation may desorb sequentially with desorption energies of  $0.60$  eV and  $0.49$  eV, respectively. The Cu species return in this way to the  $[Cu(NH_3)_2]^+$  state on which  $O_2$  may adsorb forming structure A. The adsorption energy of  $O_2$  is here calculated to be only  $0.05$  eV, which is lower than experiments and previous calculations [33]. The difference can be attributed to differences in the reference state of the initial state for the  $[Cu(NH_3)_2]^+$  pairs as well as the poor description of molecular oxygen in the used exchange-correlation functional [34].

The potential energy landscape shows the possible ways of  $NH_3$  hindering the SCR-reaction. The rate of  $NH_3$  adsorption to C is at experimentally relevant conditions lower than the rate for dissociation of B to E, thus, the system will likely transform into E and eventually G. Kinetic analysis (not shown) reveals that this is indeed the case.<sup>1</sup> The kinetic analysis explains why structure C is not observed experimentally despite the strong  $NH_3$  adsorption energy; B will dissociate before  $NH_3$  adsorbs to form C. The system will at temperatures above 423 K mainly be in state G. The probability of being in state A, which is required for the  $NH_3$ -SCR reaction has a maximum at about 473 K.

<sup>1</sup> The adsorption energy of  $O_2$  was in the kinetic analysis put to the experimental value of  $-0.82$  eV. [33]

**Fig. 4** Simulated turnover frequency for NO conversion (a) and selectivity for N<sub>2</sub> (b) over Cu-CHA as a function of temperature. The simulations are performed with 600 ppm NH<sub>3</sub>, 500 ppm NO, 10% O<sub>2</sub>, and balance N<sub>2</sub>. The red dashed line in each figure is the results from the detailed model whereas the blue line is from the simplified model

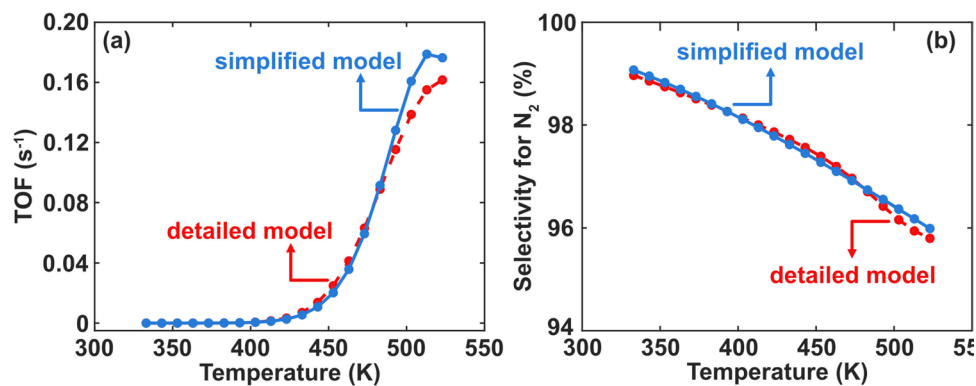


**Table 1** Original and estimated parameters for the simplified kinetic model

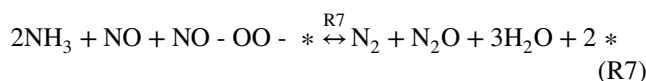
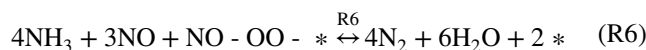
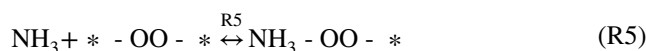
Reaction	$A_f$	$A_b$	$\Delta E_f$	$\Delta E_b$	$\Delta S_f$	$\Delta S_b$
$O_2 + 2 * \xrightleftharpoons{R3} * - OO - *$	–	–	0.13	0.33	– 134.9	17.6
$O_2 + 2 * \xrightleftharpoons{R3} * - OO - * (\text{Exp. } \Delta E)$	$8.8 \times 10^4$	$8.2 \times 10^{13}$	0.13	0.95	– 134.9	17.6
$NO + * - OO - * \xrightleftharpoons{R4} NO - OO - *$	$9.7 \times 10^4$	$9.8 \times 10^{12}$	0.00	0.70	– 109.2	0
$NH_3 + * - OO - * \xrightleftharpoons{R5} NH_3 - OO - *$	$2.2 \times 10^4$	$9.8 \times 10^{12}$	0.00	0.98	– 103.8	0
$4NH_3 + 3NO + NO - OO - * \xrightleftharpoons{R6} 4N_2 + 6H_2O + 2 *$	$9.3 \times 10^8$	–	0.34	14.1	– 14.8	–
$2NH_3 + NO + NO - OO - * \xrightleftharpoons{R7} N_2 + N_2O + 3H_2O + 2 *$	$2.4 \times 10^9$	–	0.46	10.6	– 7.0	–

Energies are given in eV and entropies in J/mol · K. The pre-exponential factors ( $A_x$ ) are given in s<sup>-1</sup> and evaluated at 473 K with 600 ppm NH<sub>3</sub>, 500 ppm NO, 10% O<sub>2</sub>, and balance N<sub>2</sub>

The detailed reaction path for NH<sub>3</sub> inhibition shows that structure E is the dominating structure at low temperatures. For the SCR reaction to proceed, E should decompose allowing for regeneration of structure A. Effectively, however, the inhibition could in a kinetic model be accounted for by considering only structure B as the NH<sub>3</sub> poisoned state.

### 3.2 Reduced Kinetic Model

In our previous work, the reaction cycle in Fig. 1 was implemented in a kinetic model [7]. The model included 18 elementary steps and it is interesting to investigate whether it could be simplified by lumping reaction steps which do not control the reaction rate. We have shown [7] that the total rate is dominated by the adsorption steps, *i.e.* O<sub>2</sub>, NO and NH<sub>3</sub> adsorption onto a pair of [Cu(NH<sub>3</sub>)<sub>2</sub>]<sup>+</sup> complexes. Here we develop a model based on the three adsorption steps and lumped reactions for N<sub>2</sub> and N<sub>2</sub>O formation:



The kinetic parameters for the elementary adsorption steps are taken from our previous study [7], whereas the parameters for the lumped reactions (R6 and R7) are determined by fitting to the detailed model. The initial values in the parameter estimation are given by the values corresponding to the highest energy barrier in the lumped reaction. The activation energies and entropy contributions from parameter estimation are listed in Table 1.

The TOF and selectivity from the simplified model is compared to the detailed model in Fig. 4. Both the TOF and selectivity for N<sub>2</sub> are in very good agreement. The onset of the reaction is at about 425 K and is associated with the desorption of NH<sub>3</sub> that blocks the Cu-site. The TOF approaches a maximum at about 525 K as the coverage of O<sub>2</sub> starts to decrease.

Phenomenological models with lumped reaction steps have previously been developed from experimental data for NH<sub>3</sub>-SCR over Cu-CHA [35]. In Ref. [35], the pre-exponential factor for the NH<sub>3</sub>-SCR reaction was reported to be  $4.83 \times 10^8 \text{ s}^{-1}$  and the corresponding activation energy to be 0.71 eV. Our model yields a comparable result for the pre-factor, which is  $9.3 \times 10^8 \text{ s}^{-1}$  for the lumped SCR-reaction (R6). However, our activation energy for R6 is 0.34 eV. The difference with respect to the phenomenological model is due to the fact that NH<sub>3</sub>-inhibition effectively was included in the SCR-reaction in Ref. [35], whereas it is treated explicitly in our model. In fact, the apparent activation energy of our simplified model is 0.76 eV, which is close to the value used in the phenomenological model. The comparison shows the advantage of a first-principles based model where the kinetic parameters can be associated with elementary reaction steps.

## 4 Conclusions

We have discussed a first-principles micro-kinetic model for low-temperature NH<sub>3</sub>-SCR over Cu-CHA. The model involves formation of H<sub>2</sub>NNO and HONO intermediates over [Cu<sub>2</sub>(NH<sub>3</sub>)<sub>4</sub>O<sub>2</sub>]<sup>2+</sup> and diffusion of the intermediates to Brønsted acid sites (NH<sub>4</sub><sup>+</sup>) where they decompose to N<sub>2</sub> and H<sub>2</sub>O. Unwanted N<sub>2</sub>O formation is accounted for by direct H<sub>2</sub>NNO decomposition over [Cu<sub>2</sub>(NH<sub>3</sub>)<sub>4</sub>OOH]<sup>2+</sup>. Here, we have analyzed in detail two crucial aspects of the model, namely how the selectivity depends on the ratio between the barriers for H<sub>2</sub>NNO diffusion and direct decomposition, and how the SCR-reaction is inhibited by NH<sub>3</sub> adsorption onto [Cu<sub>2</sub>(NH<sub>3</sub>)<sub>4</sub>O<sub>2</sub>]<sup>2+</sup> complex.

The selectivity for N<sub>2</sub> is found to be sensitive to the ratio between the barriers. The barrier for H<sub>2</sub>NNO diffusion originates mainly from the desorption from the [Cu<sub>2</sub>(NH<sub>3</sub>)<sub>4</sub>OOH]<sup>2+</sup> complex and one strategy to enhance the selectivity would be to reduce the desorption energy. The desorption energy could potentially be modified via the Al-distribution.

The micro-kinetic model shows that adsorption of extra NH<sub>3</sub> on [Cu<sub>2</sub>(NH<sub>3</sub>)<sub>4</sub>O<sub>2</sub>]<sup>2+</sup> controls the light-off temperature of the SCR reaction. We show that adsorption of two additional NH<sub>3</sub> forming [Cu<sub>2</sub>(NH<sub>3</sub>)<sub>6</sub>O<sub>2</sub>]<sup>2+</sup> is thermodynamically preferred analogous to crystal structures with the Cu<sub>2</sub>O<sub>2</sub> core coordinated to six N-ligands. However, our analysis reveals that decomposition of [Cu<sub>2</sub>(NH<sub>3</sub>)<sub>5</sub>O<sub>2</sub>]<sup>2+</sup> into [Cu(NH<sub>3</sub>)<sub>3</sub>O<sub>2</sub>]<sup>+</sup> and [Cu(NH<sub>3</sub>)<sub>2</sub>]<sup>+</sup> is kinetically preferred at relevant experimental conditions. The formation of [Cu(NH<sub>3</sub>)<sub>3</sub>O<sub>2</sub>]<sup>+</sup> and [Cu(NH<sub>3</sub>)<sub>2</sub>]<sup>+</sup> is in agreement with experimental observations [13]. [Cu(NH<sub>3</sub>)<sub>3</sub>O<sub>2</sub>]<sup>+</sup> should decompose allowing for the regeneration of the [Cu<sub>2</sub>(NH<sub>3</sub>)<sub>4</sub>O<sub>2</sub>]<sup>2+</sup> complex for the SCR reaction to proceed.

The analysis of the detailed kinetic model allows for the formulation of a simplified model for NH<sub>3</sub>-SCR with N<sub>2</sub>O formation over Cu-CHA with only five reaction steps. The simplified model was constructed with the elementary reactions for adsorption and desorption of NH<sub>3</sub>, NO and O<sub>2</sub> together with lumped reactions for N<sub>2</sub> and N<sub>2</sub>O formation. The kinetic parameters for the lumped reactions were fitted via non-linear regression. The simplified model reproduces the results for the detailed model and provides a link to a previous kinetic model developed from experimental data.

**Acknowledgements** We thank Ton V.W. Janssens, Jonas Jansson and Magnus Skoglundh for discussions and acknowledge financial support from the Swedish Energy Agency (47110-1). The Competence Centre for Catalysis (KCK) is hosted by Chalmers University of Technology and financially supported by the Swedish Energy Agency and the member companies ECAPS, Johnson Matthey, Perstorp, Powercell, Preem, Scania CV, Umicore and Volvo Group. The calculations have been performed at PDC (Stockholm) through a SNIC grant.

**Funding** Open access funding provided by Chalmers University of Technology.

**Open Access** This article is licensed under a Creative Commons Attribution 4.0 International License, which permits use, sharing, adaptation, distribution and reproduction in any medium or format, as long as you give appropriate credit to the original author(s) and the source, provide a link to the Creative Commons licence, and indicate if changes were made. The images or other third party material in this article are included in the article's Creative Commons licence, unless indicated otherwise in a credit line to the material. If material is not included in the article's Creative Commons licence and your intended use is not permitted by statutory regulation or exceeds the permitted use, you will need to obtain permission directly from the copyright holder. To view a copy of this licence, visit <http://creativecommons.org/licenses/by/4.0/>.

## References

1. Johnson TV (2014) In: Nova I, Tronconi E (eds) Review of selective catalytic reduction (SCR) and related technologies for mobile applications, pp. 3–31. Springer, New York (2014). [https://doi.org/10.1007/978-1-4899-8071-7\\_1](https://doi.org/10.1007/978-1-4899-8071-7_1)
2. Chen H-Y (2014) In: Nova I, Tronconi E (eds) Cu/zeolite SCR catalysts for automotive diesel NO<sub>x</sub> emission control, pp. 123–147. Springer, New York (2014). [https://doi.org/10.1007/978-1-4899-8071-7\\_5](https://doi.org/10.1007/978-1-4899-8071-7_5)
3. Schmiege SJ, Oh SH, Kim CH, Brown DB, Lee JH, Peden CHF, Kim DH (2012) Thermal durability of Cu-CHA NH<sub>3</sub>-SCR catalysts for diesel NO<sub>x</sub> reduction. *Catal Today* 184(1):252–261. <https://doi.org/10.1016/j.cattod.2011.10.034>
4. Xin Y, Li Q, Zhang Z (2018) Zeolitic materials for DeNO<sub>x</sub> selective catalytic reduction. *ChemCatChem* 10:29–41. <https://doi.org/10.1002/cctc.201700854>
5. Gao F, Walter ED, Kollar M, Wang Y, Szanyi J, Peden CHF (2014) Understanding ammonia selective catalytic reduction kinetics over Cu/SSZ-13 from motion of the Cu ions. *J Catal* 319:1–14. <https://doi.org/10.1016/j.jcat.2014.08.010>
6. Yao D, Liu B, Wu F, Li Y, Hu X, Jin W, Wang X (2021) N<sub>2</sub>O formation mechanism during low-temperature NH<sub>3</sub>-SCR over

- Cu-SSZ-13 catalysts with different Cu loadings. *Ind Eng Chem Res* 60(28):10083–10093. <https://doi.org/10.1021/acs.iecr.1c01514>
7. Feng Y, Wang X, Janssens TVW, Vennestrom PNR, Jansson J, Skoglundh M, Grönbeck H (2021) First-principles microkinetic model for low-temperature NH<sub>3</sub>-assisted selective catalytic reduction of NO over Cu-CHA. *ACS Catal* 14395–14407 <https://doi.org/10.1021/acscatal.1c03973>
  8. Chen L, Janssens TVW, Vennestrom PNR, Jansson J, Skoglundh M, Grönbeck H (2020) A complete multisite reaction mechanism for low-temperature NH<sub>3</sub>-SCR over Cu-CHA. *ACS Catal* 10(10):5646–5656. <https://doi.org/10.1021/acscatal.0c00440>
  9. Paolucci C, Khurana I, Parekh AA, Li S, Shih AJ, Li H, Di Iorio JR, Albarracin-Caballero JD, Yezerets A, Miller JT et al (2017) Dynamic multinuclear sites formed by mobilized copper ions in NO<sub>3</sub> selective catalytic reduction. *Science* 357(6354):898–903. <https://doi.org/10.1126/science.aan5630>
  10. Paolucci C, Parekh AA, Khurana I, Di Iorio JR, Li H, Albarracin Caballero JD, Shih AJ, Anggara T, Delgass WN, Miller JT et al (2016) Catalysis in a cage: condition-dependent speciation and dynamics of exchanged Cu cations in SSZ-13 zeolites. *J Am Chem Soc* 138(18):6028–6048. <https://doi.org/10.1021/jacs.6b02651>
  11. Paolucci C, Di Iorio JR, Schneider WF, Gounder R (2020) Solvation and mobilization of copper active sites in zeolites by ammonia: consequences for the catalytic reduction of nitrogen oxides. *Acc Chem Res* 53(9):1881–1892. <https://doi.org/10.1021/acs.accounts.0c00328>
  12. Chen L, Falsig H, Janssens TVW, Grönbeck H (2018) Activation of oxygen on (NH<sub>3</sub>-Cu-NH<sub>3</sub>)<sup>+</sup> in NH<sub>3</sub>-SCR over Cu-CHA. *J Catal* 358:179–186. <https://doi.org/10.1016/j.jcat.2017.12.009>
  13. Negri C, Selli T, Borfecchia E, Martini A, Lomachenko KA, Janssens TVW, Cutini M, Bordiga S, Berlier G (2020) Structure and reactivity of oxygen-bridged diamino dicopper(II) complexes in Cu-ion-exchanged Chabazite catalyst for NH<sub>3</sub>-mediated selective catalytic reduction. *J Am Chem Soc* 142(37):15884–15896. <https://doi.org/10.1021/jacs.0c06270>
  14. Solomon EI, Heppner DE, Johnston EM, Ginsbach JW, Cirera J, Qayyum M, Kieber-Emmons MT, Kjaergaard CH, Hadt RG, Tian L (2014) Copper active sites in biology. *Chem Rev* 114(7):3659–3853. <https://doi.org/10.1021/cr400327t>
  15. Feng Y, Janssens TVW, Vennestrom PNR, Jansson J, Skoglundh M, Grönbeck H (2021) The role of H<sup>+</sup>- and Cu<sup>+</sup>-sites for N<sub>2</sub>O formation during NH<sub>3</sub>-SCR over Cu-CHA. *J Phys Chem C* 125(8):4595–4601. <https://doi.org/10.1021/acs.jpcc.0c11008>
  16. Kresse G, Hafner J (1993) Ab initio molecular dynamics for open-shell transition metals. *Phys Rev B* 48(17):13115–13118. <https://doi.org/10.1103/PhysRevB.48.13115>
  17. Kresse G, Hafner J (1994) Ab initio molecular-dynamics simulation of the liquid-metalamorphous-semiconductor transition in germanium. *Phys Rev B* 49(20):14251–14269. <https://doi.org/10.1103/PhysRevB.49.14251>
  18. Kresse G, Furthmüller J (1996) Efficient iterative schemes for ab initio total-energy calculations using a plane-wave basis set. *Phys Rev B* 54(16):11169–11186. <https://doi.org/10.1103/PhysRevB.54.11169>
  19. Kresse G, Furthmüller J (1996) Efficiency of ab-initio total energy calculations for metals and semiconductors using a plane-wave basis set. *Comput Mater Sci* 6(1):15–50. [https://doi.org/10.1016/0927-0256\(96\)00008-0](https://doi.org/10.1016/0927-0256(96)00008-0)
  20. Perdew JP, Burke K, Ernzerhof M (1996) Generalized gradient approximation made simple. *Phys Rev Lett* 77(18):3865–3868. <https://doi.org/10.1103/PhysRevLett.77.3865>
  21. Isseroff LY, Carter EA (2012) Importance of reference hamiltonians containing exact exchange for accurate one-shot GW calculations of Cu<sub>2</sub>O. *Phys Rev B* 85(23), 1–7 (2012). <https://doi.org/10.1103/PhysRevB.85.235142>
  22. Chen L, Janssens TVW, Grönbeck H (2019) A comparative test of different density functionals for calculations of NH<sub>3</sub>-SCR over Cu-Chabazite. *Phys Chem Chem Phys* 21(21):10923–10930. <https://doi.org/10.1039/c9cp01576k>
  23. Grimme S, Antony J, Ehrlich S, Krieg H (2010) A consistent and accurate ab initio parametrization of density functional dispersion correction (DFT-D) for the 94 elements H-Pu. *J Chem Phys* 132(15):154104. <https://doi.org/10.1063/1.3382344>
  24. Grimme S, Ehrlich S, Goerigk L (2012) Effect of the damping function in dispersion corrected density functional theory. *J Comput Chem* 32:1456–1465. <https://doi.org/10.1002/jcc>
  25. Blöchl PE (1994) Projector augmented-wave method. *Phys Rev B* 50(24):17953–17979. <https://doi.org/10.1103/PhysRevB.50.17953>
  26. Kresse G, Joubert D (1999) From ultrasoft pseudopotentials to the projector augmented-wave method. *Phys Rev B* 59(3):1758–1775. <https://doi.org/10.1103/PhysRevB.59.1758>
  27. Mills G, Jónsson H, Schenter GK (1995) Reversible work transition state theory: application to dissociative adsorption of hydrogen. *Surf Sci* 324(2–3):305–337. [https://doi.org/10.1016/0039-6028\(94\)00731-4](https://doi.org/10.1016/0039-6028(94)00731-4)
  28. Henkelman G, Jónsson H (2000) Improved tangent estimate in the nudged elastic band method for finding minimum energy paths and saddle points. *J Chem Phys* 113(22):9978–9985. <https://doi.org/10.1063/1.1323224>
  29. Nosé S (1984) A unified formulation of the constant temperature molecular dynamics methods. *J Chem Phys* 81(1):511–519. <https://doi.org/10.1063/1.447334>
  30. Hoover WG (1985) Canonical dynamics: equilibrium phase-space distributions. *Phys Rev A* 31(3):1695–1697. <https://doi.org/10.1103/PhysRevA.31.1695>
  31. Chen L, Falsig H, Janssens TVW, Jansson J, Skoglundh M, Grönbeck H (2018) Effect of Al-distribution on oxygen activation over Cu-CHA. *Catal Sci Technol* 8(8):2131–2136. <https://doi.org/10.1039/c8cy00083b>
  32. Lam BMT, Halfen JA, Young VG, Hagadorn JR, Holland PL, Lledós A, Cucurull-Sánchez L, Novoa JJ, Alvarez S, Tolman WB (2000) Ligand macrocycle structural effects on copper-dioxygen reactivity. *Inorg Chem* 39(18):4059–4072. <https://doi.org/10.1021/ic000248p>
  33. Wang X, Chen L, Vennestrom PNR, Janssens TVW, Jansson J, Grönbeck H, Skoglundh M (2021) Direct measurement of enthalpy and entropy changes in NH<sub>3</sub> promoted O<sub>2</sub> activation over Cu-CHA at low temperature. *ChemCatChem* 13(11):2577–2582. <https://doi.org/10.1002/cctc.202100253>
  34. Kurth S, Perdew JP, Blaha P (1999) Molecular and solid-state tests of density functional approximations: LSD, GGAs, and meta-GGAs. *Int J Quantum Chem* 75(4–5):889–909
  35. Olsson L, Wijayanti K, Leistner K, Kumar A, Joshi SY, Kamasamudram K, Currier NW, Yezerets A (2015) A multi-site kinetic model for NH<sub>3</sub>-SCR over Cu/SSZ-13. *Appl Catal B* 174:212–224. <https://doi.org/10.1016/j.apcatb.2015.02.037>